Ph.D. Thesis

Fibroblast growth factor 10 and its receptors, FGFR2-IIIbs, are involved in skeletal development

線維芽細胞増殖因子10による骨・軟骨形成制御と
骨・軟骨由来可溶型FGFR2-IIIbの同定

Kazuko Kagawa, D.D.S.

Department of Advanced Prosthodontics
Biomedical Sciences Major
Graduate School of Biomedical & Health Sciences
Hiroshima University

Supervisor: Kazuhiro Tsuga, D.D.S., Ph.D.

2015

ACKNOWLEDGEMENTS

APPENDIX

A part of this study was presented in the following meetings:

1. 胎生期中後期における線維芽細胞増殖因子（FGF）10の過剰発現はマウス頭蓋顎顔面の形成障害をもたらす．The 56th Annual Meeting of Japanese Association for Oral Biology. Fukuoka, Sep. 2014.

2. 線維芽細胞増殖因子（FGF）10がマウスの頭蓋顎顔面形態形成に与える影響．The 69th Chugoku-Shikoku Sectional Meeting of Japanese Association of Anatomists. Hiroshima, Oct. 2014.

3. 線維芽細胞増殖因子（FGF）10は頭蓋顎顔面の骨格形成を負に制御する．The 98th Annual Meeting of the Hiroshima University Dental Society. Hiroshima, Nov. 2014.

4. 線維芽細胞増殖因子（FGF）10による骨・軟骨形成制御と骨・軟骨由来可溶型FGFR2bの同定．先端歯学スクール2015. Fukuoka, Sep. 2015.

5. Newly Identified FGFR2 Isoform Modulates FGF10-FGFR Signaling During Osteochondrogenesis. The American Society for Bone and Mineral Research 2015 Annual Meeting. Seattle, Oct. 2015.

6. A Novel isoform of FGFR2 Modulates FGF10-FGFR Signaling in Osteochondrogenesis. 6th Hiroshima Conference on Education and Science in Dentistry. Hiroshima, Oct. 2015

CONTENTS

I. ABSTRACT

The fibroblast growth factor (FGF) family consists of 18 members and plays a key role in many aspects of development, such as cell proliferation and differentiation through FGF receptor (FGFR) tyrosine kinases and their coupled intracellular signaling pathways. Gain-of-function mutations in a common extracellular domain of FGFR2 isoforms (types IIIb and IIIc) cause craniosynostosis and chondrodysplasia syndromes. FGF10, a major ligand for FGFR2-IIIb, is secreted from mesenchymal cells and acts on epithelial cells as a mediator of epithelial-mesenchymal interactions. Meanwhile, FGF10 appears to act on mesenchymal cells and regulate preadipocyte differentiation and early chondrogenesis. These results led us to hypothesize that FGF10-FGFR signaling is involved in bone and/or cartilage formation. To test this hypothesis, transgenic (TG) mice expressing mouse FGF10 under the control of doxycycline were generated. Compared with control littermates, TG pups overexpressing FGF10 from embryonic day 12.5 were small in body size and had a short cranium in the rostrocaudal axis. Whole-mount skeletal staining and micro-CT revealed skeletal dysplasia including shorter long bones, dwarfed mandibles, developmental retardation in the mandibular condylar cartilage, and cleft palate. In an analysis of the causal link between FGF10 and FGFR2, the additional alternative splicing variant of *Fgfr2-IIIb* expressed particularly in the bone, cartilage, and mouse prechondrogenic ATDC5 cells was found. The predicted translation product of this variant appears to include both exon 8- and 9-encoded residues (types IIIb and IIIc, respectively) and lack membrane-spanning and tyrosine kinase domains, suggesting a soluble form of FGFR2-IIIb (sFGFR2-IIIb). sFGFR2-IIIb was identified in the conditioned media of ATDC5 cells, and the overexpression of sFGFR2-IIIb increased cell proliferation, suggesting that sFGFR2-IIIb may modulate FGF signaling. Thus,

a large amount of FGF10 may trap sFGFR2-IIIb and allow the increased activation of other

FGF-FGFR signaling pathways, resulting in skeletal anomalies in TG mice.

II. INTRODUCTION

Skeletal development requires highly organized signaling systems that coordinate with the various types of cells to form various components such as the bone, cartilage, and joints at an appropriate time and location (Kobayashi and Kronenberg, 2014; Berendsen and Olsen, 2015). Fibroblast growth factor (FGF) and fibroblast growth factor receptor (FGFR) signaling is one of the important signaling pathways for the regulation of skeletogenesis (Su *et al*., 2014; Ornitz and Marie, 2015). Eighteen members of the FGF family have been identified so far and can be grouped into six subfamilies by their distinct paracrine or hormonal actions (Beenken and Mohammadi, 2009; Goetz and Mohammadi, 2013). FGFs mediate their biological processes by binding and activating the tyrosine kinase receptors (FGFR1-4), following the activation of the Ras-mitogen-activated protein kinase pathways, phosphatidylinositol 3-kinase-Akt pathway, and phospholipase Cγ-protein kinase C pathway (Beenken and Mohammadi, 2009; Goetz and Mohammadi, 2013). Overall, by activating these signaling pathways, FGFs play a crucial role in the control of cell migration, proliferation, differentiation, and survival (Beenken and Mohammadi, 2009; Goetz and Mohammadi, 2013).

FGFRs are encoded by four distinct genes (*Fgfr1-4*) and are characterized by two or three extracellular immunoglobulin (Ig)-like loops, a single transmembrane domain, and a cytoplasmic tyrosine kinase domain (Beenken and Mohammadi, 2009; Goetz and Mohammadi, 2013). Variation in ligand binding specificity is achieved by alternative splicing of the exons encoding the third Ig-like loops in *Fgfr1-3*, which generates IIIb or IIIc isoforms (Beenken and Mohammadi, 2009; Goetz and Mohammadi, 2013). Mutations of these FGFRs skew the ligand binding specificity and constitutively activate these receptors in a

ligand-independent manner, causing chondrodysplasia and craniosynostosis cases, including Apert, Crouzon, and Pfeiffer syndromes. These mutations exist in the common extracellular domain of FGFR isoforms (IIIb and IIIc) suggesting that a net gain of FGFR function contributes to the pathogenesis of these syndromes (Ornitz, 2005). This is supported by the fact that the abrogation of FGF10 in an Apert syndrome mouse model rescues their skeletal defects (Hajihosseini *et al*., 2009). FGF10 is well-known mesenchymal factor and functions in epithelial-mesenchymal interaction via its local secretion to bind to specific receptors, FGFR2-IIIb and FGFR1-IIIb, on epithelial tissues (Zhang *et al*., 2006; Itoh, 2015). Knockout animal models of both *Fgf10* and *Fgfr2-IIIb* are viable until birth and show similar deformities of many epithelial organs such as the limb, lung, salivary gland, and palate (Sekine *et al*., 1999; De Moerlooze *et al*., 2000). The functional significance of FGF10 in the mesenchymal tissues has also been reported. FGF10 is abundant in white adipose tissue and regulates the proliferation and differentiation of preadipocytes (Sakaue *et al*., 2002). In an *in vitro* experiment, FGF10 inhibits the cell proliferation of growth plate chondrocytes (Olney *et al*., 2004). In an *ex vivo* experiment, the overexpression of *Fgf10* in the developing mandibles is shown to enhance chondrogenic differentiation (Terao *et al*., 2011). However, conflicting data show that FGF10 does not affect either proliferation or differentiation in cultures of osteoblasts, osteoclasts, and chondrocytes (Shimoaka *et al*., 2002). Therefore, the impact of FGF10 on bone and cartilage development remains unclear.

In this study, a Tet-on doxycycline (Dox)-inducible transgenic mouse model was used to study the role of FGF10 in bone and cartilage development after the formation of bone and cartilage primordia. Limb skeletal development starts as mesenchymal condensations, with the subsequent formation of cartilage anlagen from approximately embryonic day (E) 11.5 to 13.5 (Kaufman, 1992). Craniofacial skeletogenesis is first observed in the chondrocranium as

parachordal cartilage formation at E11 and then expands to form the canalicular part of the auditory capsule and occipital arch cartilage at E12 (McBratney-Owen *et al*., 2008). Condensed mesenchymal pharyngeal arch cartilage also starts to form at E12 (Kaufman, 1992). Considering these developmental time points, pregnant mice were fed Dox from E12.5. Then, histopathological and molecular biological analyses were performed to determine the effect of enforced FGF10 expression in the embryos (E18.5) and newborn pups. These results show the possible contribution of FGF10 to bone and cartilage formation. A novel soluble form of FGFR2-IIIb (sFGFR-IIIb) that generally exists in the bone and cartilage was also identified. Taken together, these findings indicate that the possible interaction of FGF10 and sFGFR-IIIb may regulate the development of bone and cartilage.

III. MATERIALS AND METHODS

3-1. Generation of rtTA; tet(O)Fgf10 mice

The transgenic mice constitutively expressing CMV-rtTA were purchased from the Jackson laboratory (Parsa *et al*., 2010). This constitutive CMV-rtTA mouse line was crossed with the tet(O)Fgf10 (Clark *et al*., 2001), which was kindly provided by Dr. JA Whitestt (Cincinnati Children's Hospital Medical Center, OH, USA), allowing the ubiquitous expression of *Fgf10*. All mice were conventionally reared and fed a regular diet. The mice were genotyped as described on the website of the Jackson laboratory (http://www.jax.org/index.html). To obtain the *Fgf10*-overexpressing (CMV-rtTA tg/+;tet(o)Fgf10 tg/tg and/or CMV-rtTA tg/+;tet(o)Fgf10 tg/+) and -non-overexpressing (tet(o)Fgf10 tg/tg and/or tet(o)Fgf10 tg/+) control embryos as littermates, tet(o)Fgf10 tg/tg female mice were bred with CMV-rtTA tg/+;tet(o)Fgf10 tg/+ male mice. Mating was assessed by the presence of a vaginal plug on the following morning, and recorded as embryonic day 0.5 (E0.5). The expression of *Fgf10* was induced in pregnant mice by replacing normal drinking water with 5% sucrose containing 2 mg/ml of doxycycline hyclate (Dox; Sigma-Aldrich, St Louis, MO) from E12.5. Dox reaches the embryo by 4 h at the earliest and 24 h at the latest (Kistner *et al*., 1996). It should be noted that the pregnant mice were not affected by the consumption of Dox. Five animals were used for each of the control and experimental groups. Animal use and procedures were approved by the Committee of Animal Experimentation at Hiroshima University.

3-2. Micro-CT (μCT) analysis

The newborn pups were scanned in a μCT under the following conditions: tube voltage, 40 kV; tube current, 600 μA; image pixel size, 17.5 μm; and no filter. The images were reconstructed using NRecon (Skyscan).

3-3. Whole-mount skeletal preparation

Whole-mount skeletal preparations of newborn mice were performed as described previously (Kimmel and Trammell, 1981). In brief, skinned and eviscerated specimens were stained with 0.14% Alcian blue and 0.12% Alizarin red S in ethanol and glacial acetic acid. Then, the specimens were cleared in 2% KOH and stored in 1:1 mixture of glycerin and distilled water.

3-4. Preparation of tissue sections and immunohistochemistry

Embryos were fixed in 4% paraformaldehyde overnight at 4°C and demineralized in 10% EDTA-PBS for a few days. These samples were then dehydrated and embedded in paraffin. Deparaffinized sections (5 μm thick) were subjected to standard hematoxylin-eosin (HE) and tartrate-resistant acid phosphatase (TRAP) staining as well as immunohistochemical staining. For immunohistochemistry, to detect type X collagen, sections were pretreated with 0.1% hyaluronidase in TBS (20 mM Tris-HCl pH 7.6, 150 mM NaCl) for 1 h at 37˚C. Sections were then incubated with Protein Block (DAKO, Glostrup, Denmark) for 30 min and subsequently with primary antibodies against type X collagen (1:1000, Cosmo Bio, Tokyo, Japan) and alkaline phosphatase (ALP; 1:100, ProteinTech, Chicago, IL) overnight at 4˚C. Alexa Fluor 594 goat anti-rabbit IgG (1:500; Life Technologies, Carlsbad, CA) was used as a secondary antibody (1 h at room temperature). Negative control experiments were performed using normal rabbit IgGs at the same concentration as the primary antibody. The slides were mounted in Vectashield with DAPI (Vector Laboratories, Burlingame, CA), and signals were

observed under a Leica DMI 4000B inverted fluorescence microscope (Leica Microsystems, Wetzlar, Germany).

3-5. Expression analysis

Total RNA was isolated using TriPure Isolation Reagent (Roche Diagnostics, Indianapolis, IN). First-strand cDNA synthesis was performed using ReverTraAce, in accordance with the manufacturer's instructions (Toyobo, Osaka, Japan). General PCR was performed with KOD Fx Neo polymerase (Toyobo) using the gene-specific primers. The reaction products were analyzed by electrophoresis in a 2% agarose gel and stained with ethidium bromide (Wako Pure Chemical Industries, Osaka, Japan). Quantitative real-time PCR was performed using the StepOnePlus real-time PCR system (Life Technologies) with Fast SYBR Green Master Mix (Life Technologies). PCR primer sets were as follows: for *Fgfr2-IIIb*, 5′-CTC ACT GTC CTG CCC AAA CA-3′, 5′-CAC CAT GCA GGC GAT TAA GA-3′; for *Fgfr2-IIIc*, 5′-GCT TCA TCT GCC TGG TCT TGG-3′, 5′-TGG GAG ATT TGG TAT TTG GTT GG-3′; for *Fgf10*, 5′-AGC GGG ACC AAG AAT GAA G-3′, 5′-GCT GTT GAT GGC TTT GAC G-3′; for *Sox9*, 5′-CTA TCT TCA AGG CGC TGC AA-3′, 5′-GTC GGT TTT GGG AGT GGT G-3′; for *Runx2*, 5′-TTC TGC CTC TGG CCT TCC TC-3′, 5′-AAG GGC CCA GTT CTG AAG CA-3′; for *Col2a1*, 5′-GTG GAG CAG CAA GAG CAA GG-3′, 5′-CTG GAC GTT AGC GGT GTT GG-3′; for *Col10a1*, 5′-GGC AGA GGA AGC CAG GAA AG-3′, 5′-TTA GCA GCA GAA AGG GTA TTT GAG G-3′; and for ß-actin (*Actb*), 5′-GGC TGT ATT CCC CTC CAT CG-3′, 5′-GCC TCG TCA CCC ACA TAG GA-3′ (forward and reverse, respectively). The results were normalized against the reference *Actb* gene.

3-6. Expression vectors

The coding sequence of soluble-type FGFR2-IIIb (sFGFR2-IIIb) was amplified by KOD-Plus-Neo using primers containing restriction sites for *Xba*I and *Hind*III (underlined) in forward (5′-AGG CTC TAG AGT CTC AGA AGA AGT GTG CAG-3′) and reverse (5′-ATT AAG CTT GAC ACC GGC GGC TTG CT GTT-3′), respectively, and was inserted into the pcDNA3.1/myc-His(-) expression vector at the appropriate restriction sites. The insert was confirmed by DNA sequencing.

3-7. Cell culture, transfection, and MTT assay

The mouse prechondrogenic cell line ATDC5 was cultured in a 1:1 mixture of DMEM and Ham's F-12 medium (DMEM/F12; Wako Pure Chemical Industries, Osaka, Japan) containing 5% fetal calf serum and antibiotics at 37°C and 5% CO_2. ATDC5 cells were transfected with the *sFgfr2-IIIb* expression vector or pcDNA3.1/myc-His(-) empty vector using Lipofectamine 3000 (Life Technologies), in accordance with the manufacturer's instructions. Two days after transfection, G418 (200 µg/ml, Nacalai Tesque, Kyoto, Japan) was added to the culture medium to isolate stable clones. Cell proliferation was determined by 3-[4,5-dimethylthiazol-2-yl]-2,5-diphenyltetrazolium bromide (MTT; Sigma-Aldrich, St Louis, MO) assay. The formed formazan was dissolved in dimethyl sulfoxide, and the absorbance was measured at 570 nm with a microplate reader.

3-8. Detection of soluble FGFR2-IIIb

When the ATDC5 cells reached full confluence, the culture medium was switched to serum-free DMEM/F12 supplemented with insulin, transferrin, and sodium selenite (ITS; Roche Diagnostics). Following one or two days of culture, the conditioned medium was gently rocked with heparin-Sepharose (Abcam, Cambridge, MA) at 4°C overnight. The Sepharose was then washed three times with phosphate buffer pH 7.4 and boiled with

Laemmli sample buffer for 5 min. The eluate was directly subjected to SDS-PAGE and transferred to PVDF membranes. Membranes were then incubated in a blocking solution (0.1% Tween 20, 0.1 M NaCl, 0.1 M Tris–HCl pH 7.5, and 0.2% casein) for 1 h, followed by incubation with anti-Bek antibody (1:200; Santa Cruz Biotechnology, Santa Cruz, CA, Cat. # Sc-20735) at 4˚C overnight. HRP-conjugated secondary antibody (for 1 h at room temperature; 1:1000, Santa Cruz Biotechnology) and ECL Select Western Blotting Detection System (GE Healthcare Japan, Tokyo, Japan) were used for chemiluminescence detection.

3-9. Statistical analysis

Data obtained from at least three samples are expressed as the mean ± SD. A minimum two independent experiments were performed. Statistical analyses were performed using Student's *t*-test.

IV. RESULTS

4-1. Skeletal anomalies in Fgf10-overexpressing mice

Fgf10-overexpressing (TG) mice were viable until birth, but died soon after birth probably because of the failure of lung formation (Gonzaga *et al*., 2008). They had a thin and shiny skin and characteristic craniofacial shapes, such as a shorter rostrum and mandibles in the rostrocaudal axis (Fig. 1A). The skeletons from newborn pups were stained with Alizarin red and Alcian blue to identify bone and cartilage structures, respectively (Fig. 1B-E). TG mice showed the hypoplasia of limb bones and no mineralized phalanges (Fig. 1B). TG mice also showed cleft palate and no tympanic ring formation (Fig. 1D). Furthermore, cartilage dysplasia was also observed in the frontonasal cartilage, mandibular condylar cartilage, mandibular angular cartilage, and the rostral process of Meckel's cartilage (Fig. 1C-E).

Then, newborn TG and littermate control mice were scanned using micro-CT (μCT) and reconstructed the images in 3D. The hypoplasia of neurocranial bones was found, such as the parietal bone, interparietal bone, supraoccipital bone, and exoccipital bone (Fig. 2A). Growth retardations were seen in the limb bones and phalanges (Fig. 2A). To characterize the morphology of the skull and limb bones, linear measurements were performed using the μCT images. Cranial length, cranial width, and mandibular length were significantly shorter, but the palatal width was significantly greater, in TG mice than in control (Fig. 2B). In addition, TG had significantly shorter limb bones than control (Fig. 2C). These results demonstrate that the skeletal structure of TG mice is consistently different from that of the control littermates.

4-2. Histopathological analysis of skeletal anomalies in Fgf10-overexpressing mice

Histopathological analysis of the craniomaxillofacial tissues in TG mice showed various anomalies (Fig. 3A, G). The epithelial tissue was one of the most affected tissue structures, with a keratinization defect (Fig. 3B, H), an invaginated epithelium (Fig. 3C, I), and hyperplastic exocrine glands (Fig. 3D, J). The mesenchymal tissues also showed various anomalies such as hyperplasia of the adipose tissue (Fig. 3E, K) and hyperplasia of the cartilages around the nasal septum, nasal concha, and cranial base (Fig. 3F, L). This cartilage hyperplasia is contrary to what was found from skeletal phenotypes such as hypoplasia of the mandibular condylar cartilage (Fig. 1).

Next, the bone and cartilage tissues, such as the lower limb and mandibular condyle, were focused on for a further analysis of the effect of FGF10 on skeletogenesis (Figs. 4, 5). The femurs and tibiae of TG mice tended to be narrower (Fig. 4A, D, E, H). Immunostaining of type X collagen, a marker of hypertrophic chondrocytes, demonstrated a reduction of the hypertrophic chondrocyte layer in TG tibiae (Fig. 4B, F). Alkaline phosphatase (ALP) immunostaining and tartrate-resistant acid phosphatase (TRAP) staining revealed the tendency of reduction of osteoblasts and osteoclasts number, respectively, in TG femurs (Fig. 4C, D, G, H). Analogous to the lower limbs, hypertrophic cells were hardly found (Fig. 5A, B), and the type X collagen-positive hypertrophic zone was noticeably reduced (Fig. 5C, D) in the mandibular condylar cartilage of TG mice. To characterize the molecular events leading to hypoplastic condyle, the expression levels of chondrogenesis-related genes between control and TG mandibular condylar cartilages were compared (Fig. 5E). By Dox treatment, the expression level of the *Fgf10* gene was increased 73.3-fold on average. Among the genes analyzed, the expression levels of *Runx2* and *Col10a1* were elevated and reduced, respectively, in TG condyle. Taken together, these results indicate that the excess amount of FGF10 inhibits the terminal differentiation process of chondrocytes.

4-3. Expression profiles of Fgf10 and receptors Fgfr2-IIIb and Fgfr2-IIIc in mouse tissues

To understand the mechanism underlying the regulation of osteochondrogenesis by FGF10 signaling, the expression profiles of *Fgf10*, *Fgfr2-IIIb*, and *Fgfr2-IIIc* genes were analyzed in many tissues of the wild-type newborn mice and prechondrogenic cell line ATDC5 (Fig. 6A). These genes were expressed in most of the tissues studied and ATDC5 cells. The expression analysis of *Fgfr2-IIIb* yielded an unexpected longer product in ATDC5 cells and especially in cartilage and bone tissues where the dysplasia occurred in TG mice (Figs. 1, 2). Sequence analysis revealed that this product had both exon 8 and 9 encoding IIIb and IIIc, respectively, indicating a novel alternative splicing variant of *Fgfr2-IIIb*. The inclusion of exon 9 in *Fgfr2-IIIb* mRNA changed the reading frame and resulted in the insertion of a stop codon soon after the immunoglobulin (Ig)-like domain III (Fig. 6B). Consequently, a truncated version of FGFR2-IIIb that lacks the transmembrane and tyrosine kinase domains may be produced and secreted as a soluble form. Indeed, the soluble form of FGFR2-IIIb (sFGFR2-IIIb) was detected in the conditioned media of ATDC5 cells (Fig. 6C). FGF10 was also secreted from ATDC5 cells (Fig. 6D).

4-4. The effect of soluble FGFR2-IIIb overexpression in ATDC5 cells

To evaluate the function of sFGFR2-IIIb, an expression vector to overexpress sFGFR2-IIIb in ATDC5 cells was constructed. During the process of expression vector construction, three types of sFGFR2-IIIb variants were identified (data not shown). These are the complete form, a variant that lacks exon 3 (encoding IgI), and one that lacks exon 3 and exon 4 (encoding an acid box). The complete form of sFGFR2-IIIb was used for further analysis. Two ATDC5 cell clones stably overexpressing sFGFR2-IIIb were isolated, as analyzed by real-time PCR and Western blotting analyses (Fig. 7A, B). These cells showed the acceleration of cell

proliferation in a dose-dependent manner (Fig. 7C). Thus, sFGFR2-IIIb may modulate

FGF10 and/or other FGF signaling.

V. DISCUSSION

In this study, the enforced expression of *Fgf10* in mouse embryos induced multiple malformations of tissue structures including the bone and cartilage. The cause of these malformations is assumed to be direct or indirect actions of FGF10. In addition, given the phenotypes of *Fgf10* knockout mice, dose sensitivity and dependency on FGF10 seemingly differ among the tissues. Malformations of the lung and palate in mice overexpressing and/or lacking FGF10 were similarly observed in this study (Sekine *et al*., 1999; De Moerlooze *et al*., 2000; Gonzaga *et al*., 2008). Because the fundamental mechanisms governing the morphogenesis of these tissues are the epithelial-mesenchymal interactions and the concentration gradient of FGF10 (Shannon and Hyatt, 2004; Balasubramanian and Zhang, 2015), it seems that the FGF10 has indirect and dose-sensitive effects on these tissues. Meanwhile, the direct and dose-dependent effects of FGF10 were observed in the epithelium, including gland, and adipose tissues. FGF10 stimulates the proliferation of epithelial cells in a direct manner (Igarashi *et al*., 1998; Marchese *et al*., 2001). Therefore it is speculated that the abundant FGF10 accelerates epithelial cell proliferation and impedes the differentiation process, leading to loss of the cornified layer and hyperplasia of glands (Fig. 3). FGF10 also coordinates the proliferation of preadipocytes and differentiation process of adipogenesis by activating CEBP/α and PPARγ (Ohta and Itoh, 2014). Hence, the excess FGF10 could facilitate the proliferation and differentiation of preadipocytes, leading to the hyperplasia of adipose tissues (Fig. 3). In addition to these etiologies, the possible competition between FGF10 and other FGFs for binding to the common FGF receptor may cause the malformations of tissue structures in TG. The abundant FGF10 may inhibit the binding of FGF3, a main contributor of tympanic ring formation (Mansour *et al*., 1993), to the common

receptor FGFR2-IIIb and, as a consequence, the tympanic ring does not form in TG (Fig. 1D).

The two opposite phenomena, hypoplasia and hyperplasia, were observed in different cartilage regions of TG mice. Immunohistochemical and gene expression analyses revealed that cartilage hypoplasia was caused by the inhibition of differentiation into hypertrophic chondrocytes (Figs. 4, 5). However, the expression of *Runx2*, a transcription factor required for chondrocyte differentiation, was elevated (Fig. 5E). This is probably because of more complex functions of *Runx2* during chondrogenesis. *Runx2* is expressed in prehypertrophic chondrocytes and triggers hypertrophy of chondrocytes by activating *Ihh* and *Col10a1* (Zheng *et al*., 2003; Yoshida *et al*., 2004). On the other hand, long-lasting perichondrial expression of *Runx2* inhibits chondrocyte proliferation and hypertrophy (Hinoi *et al*., 2006). This negative effect on chondrogenesis may predominantly act and affect endochondral ossification resulting in the reduction of osteoblast number in long bones of TG (Fig. 4C, G). The reduction of osteoblast number may also be due in part to decreased transdifferentiation of hypertrophic chondrocytes into osteoblasts and osteocytes (Yang *et al*., 2014; Zhou *et al*., 2014). The abundance of FGF10 affected not only endochondral ossification but also intramembranous ossification (Figs. 1, 2). *Fgf10* is expressed in osteoprogenitors of the frontal bone during development, suggesting that FGF10 acts directly on osteogenesis (Veistinen *et al*., 2009). However, there is still a need to clarify the molecular mechanisms underlying the effects of FGF10 on osteoblast and osteoclast differentiation.

A novel soluble form of FGFR2-IIIb (sFGFR2-IIIb) was identified in some bones and cartilage (Fig. 6). The overexpression of *sFgfr2-IIIb* increased the proliferation of ATDC5 cells (Fig. 7), indicating that the sFGFR2-IIIb has some function in regulating the activity of

signal transduction. One possibility is as a decoy receptor. The extracellular sFGFR2-IIIb may trap FGF10 and other FGF subfamilies, such as FGF3, FGF7, and FGF22, and modulate the signal activity by sequestering the binding to the membranous type of FGFRs. The other possibility is that the sFGFR2-IIIb forms a heterocomplex with other receptors. Considering the fact that FGFR2 forms heterodimers with FGFR1 *in vitro* (Wang *et al*., 1997), heterodimerization of sFGFR2-IIIb with FGFR1 or other receptors could have a unique function by transducing a unique signaling pathway. In TG mice, the bone and cartilage where *sFgfr2-IIIb* was expressed showed hypoplasia. In contrast, the bone and cartilage expressing the membranous-type *Fgfr2-IIIb* showed either hyperplasia or no phenotypes (Figs. 1, 2, 6A). These observations indicate that sFGFR2-IIIb contributes to the etiology of hypomorphic structures of the bone and cartilage in TG mice. The abundant FGF10 may trap sFGFR2-IIIb and allow the transduction of extraordinary signaling activity by the escaped FGF10 and/or other FGFs. The membranous type of FGFR2-IIIb is not expressed in the tissues that showed hypoplasia in TG mice (Figs. 1, 2, 6A), indicating that FGF10 binds to the second receptor, FGFR1-IIIb. FGFR1 is expressed in prehypertrophic and hypertrophic chondrocytes and regulates the terminal maturation of hypertrophic chondrocytes (Jacob *et al*., 2006). Taken together, excess FGF10-FGFR1 signaling may inhibit the process of chondrocyte differentiation. Indeed, constitutive FGFR1 activity causes osteoglophonic dysplasia, characterized by multiple osteochondrogenic anomalies such as rhizomelic dwarfism, craniosynostosis, and low bone mineral density (White *et al*., 2005). FGF10 is also a key factor for epithelial-mesenchymal interaction and induces the expression of FGF8 in the ectodermal tissues (Itoh, 2015). FGF8 has promotive effects on chondrogenesis during cranial development (Abzhanov and Tabin, 2004). The abundant FGF8 may be induced by excess FGF10 and accelerate the growth of cartilage in the nasal septum, nasal concha, and cranial base (Fig. 3).

Thus, the large amount of FGF10 in TG mice may modulate multiple FGF-FGFR signaling pathways, resulting in skeletal anomalies. Above all, because a variety of skeletal elements are involved in craniomaxillofacial development, the remarkable effect of FGF10 overexpression on the region may be closely related to the mixed system in the presence and absence of sFGFR2-IIIb.

Figure 1. Skeletal anomalies in *Fgf10*-overexpressing mice. (A) Gross appearance of newborn mice. (B-E) Skeletons of newborn mice stained with Alizarin red and Alcian blue. The top (C) and basal (D) views of the craniomaxillofacial skeletons. The mandibles were removed to enhance the view of the cranial base. Tympanic rings (arrowheads) were observed in control mice, but not in TG mice. Cleft palate (arrow) was observed in TG mice. (E) The lateral view of the mandibles. Scale bars = 5 mm.

Figure 2. μCT analysis of bone anomalies in *Fgf10*-overexpressing mice. (A) Three-dimensional reconstructions from μCT images of newborn control (upper panel) and TG mice (lower panel). Whole skeletons (left) and lateral (middle) and basal (right) views of the craniomaxillofacial skeletons are shown. The mandibles were removed to enhance the view of the cranial base. Morphological assessments of the craniomaxillofacial skeletons (B) and long bones (C) were performed by linear measurements. Landmarks, a-h in the left panel of (B), were used to assess linear measurements of the craniofacial structures. n = 10 per group; **, *P* < 0.01.

Figure 3. Histological anomalies in the epithelial and mesenchymal structures of *Fgf10*-overexpressing mice. Coronal sections of HE-stained craniomaxillofacial structures in control (A-F) and TG (G-L) embryos. Higher magnifications of the areas enclosed by solid lines in (A) and (G) are shown in (B-E) and (H-K), respectively. The skin (B, H), tongue (C, I), nasal gland (D, J), and adipose tissue (E, K) are shown. The areas enclosed by dotted lines in (A) and (G) are shown in (F) and (L), respectively. The cartilages around the nasal septum,

nasal concha, and cranial base are shown (F, L). Scale bars = 500 μm in A, F, G, L and 100 μm in B-E, H-K.

Figure 4. Histological anomalies in the long bones of *Fgf10*-overexpressing mice. Longitudinal sections of tibiae (A, B, E, F) and femurs (C, D, G, H) were stained with HE (A, E) and TRAP (D, H) and immunostained with type X collagen (B, F; red) and ALP (C, G; red). The nuclei were stained with DAPI (B, C, F, G; blue). Arrowheads indicate the ALP-positive cells (an osteoblast marker; C, G) and TRAP-positive cells (an osteoclast marker; D, H). Scale bars = 200 μm.

Figure 5. Histological and gene expression anomalies in the mandibular condylar cartilage of *Fgf10*-overexpressing mice. Coronal sections of HE-stained (A, B) and type X collagen-immunostained (C, D) condylar cartilage in control (A, C) and TG (B, D) embryos. (A, B) Higher magnifications of the areas enclosed by solid lines in the left panels are shown in the right panels. (C, D) The areas enclosed by solid lines in the left panels (phase contrast) correspond to the areas of immunostaining of type X collagen (red, right panels). DAPI (blue) was used for nuclear staining. Scale bars = 500 μm in the left panels of A, B; 200 μm in the right panels of A, B; and 100 μm in C, D. (E) Quantitative expression profiles of *Fgf10* and chondrogenic genes in the mandibular condylar cartilage. The relative amount of each target mRNA in the control was arbitrarily set at 1, and all other transcript levels were compared with this value. The results of three independent experiments are shown for the *Fgf10* gene. *, $P < 0.05$.

Figure 6. Detection of the soluble form of FGFR2-IIIb. (A) Expression profiles of *Fgfr* and *Fgf10* genes in normal mouse tissues and the prechondrogenic cell line ATDC5.

Representative images of agarose gel electrophoresis of RT-PCR products are shown. The ß-actin gene (*Actb*) was also amplified as an internal control. (B) Schematic structures of FGFR2 and soluble FGFR2-IIIb (sFGFR2-IIIb). Detection of sFGFR2-IIIb (C) and FGF10 (D) in the heparin bound fraction of conditioned media by Western blotting. Conditioned media were collected after incubation for one or two days.

Figure 7. Acceleration of ATDC5 cell proliferation by overexpressing sFGFR2-IIIb. Real-time PCR (A) and Western blotting (B) analyses confirmed the overexpression of sFGFR2-IIIb in two clones (OE-1 and OE-2). (C) Cell proliferation analysis by MTT assay. *, $P < 0.05$; **, $P < 0.01$ vs. control.
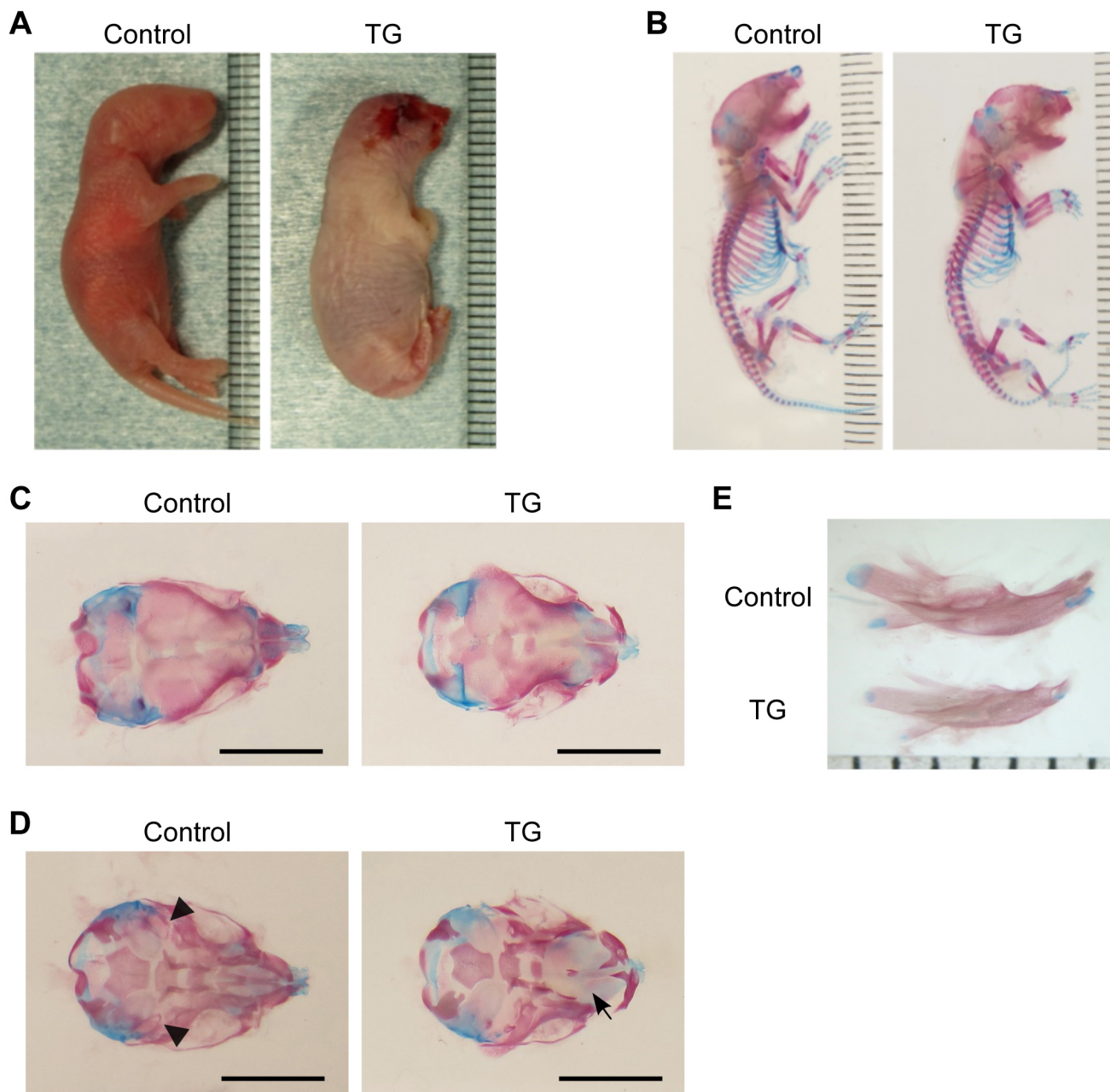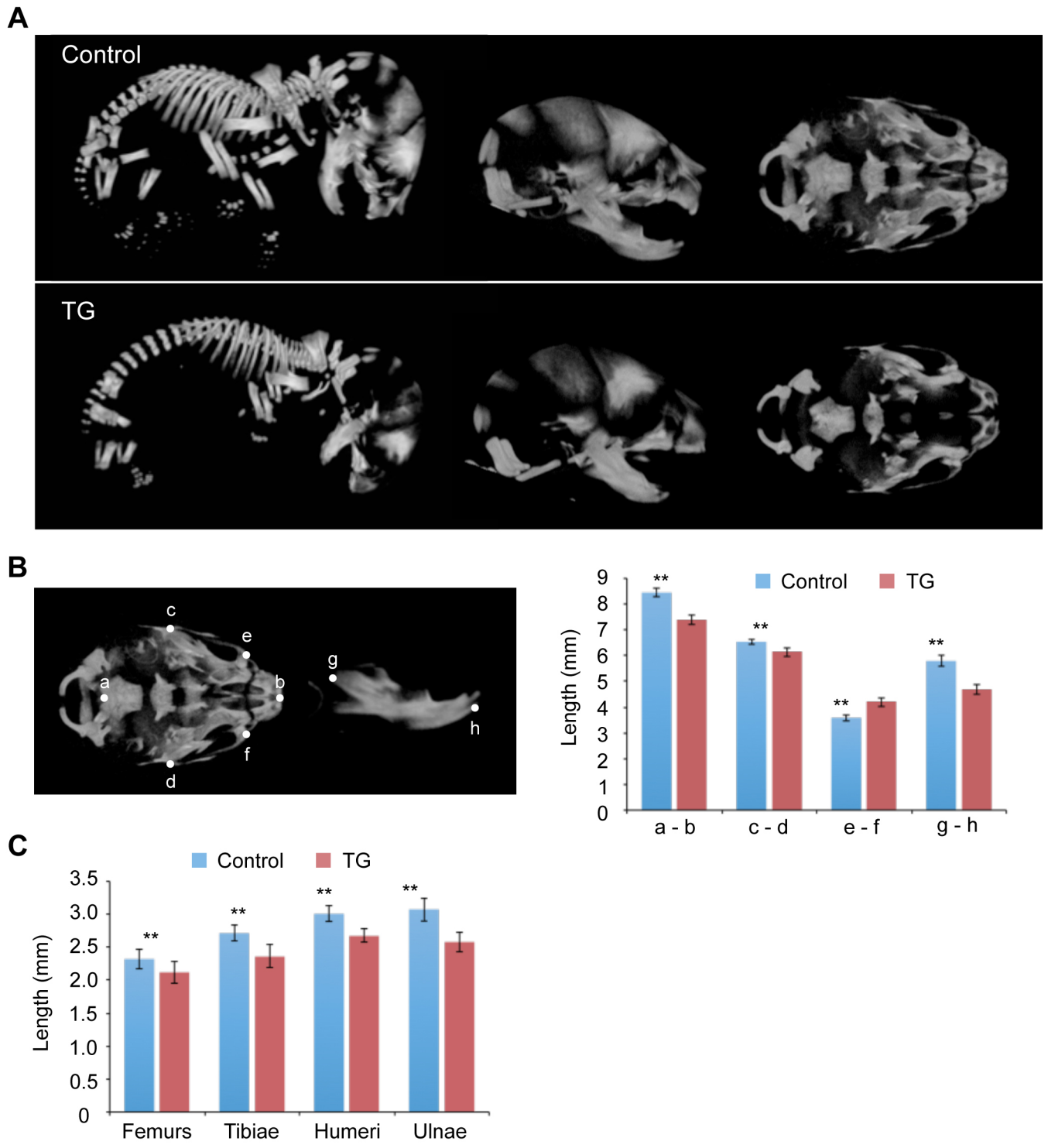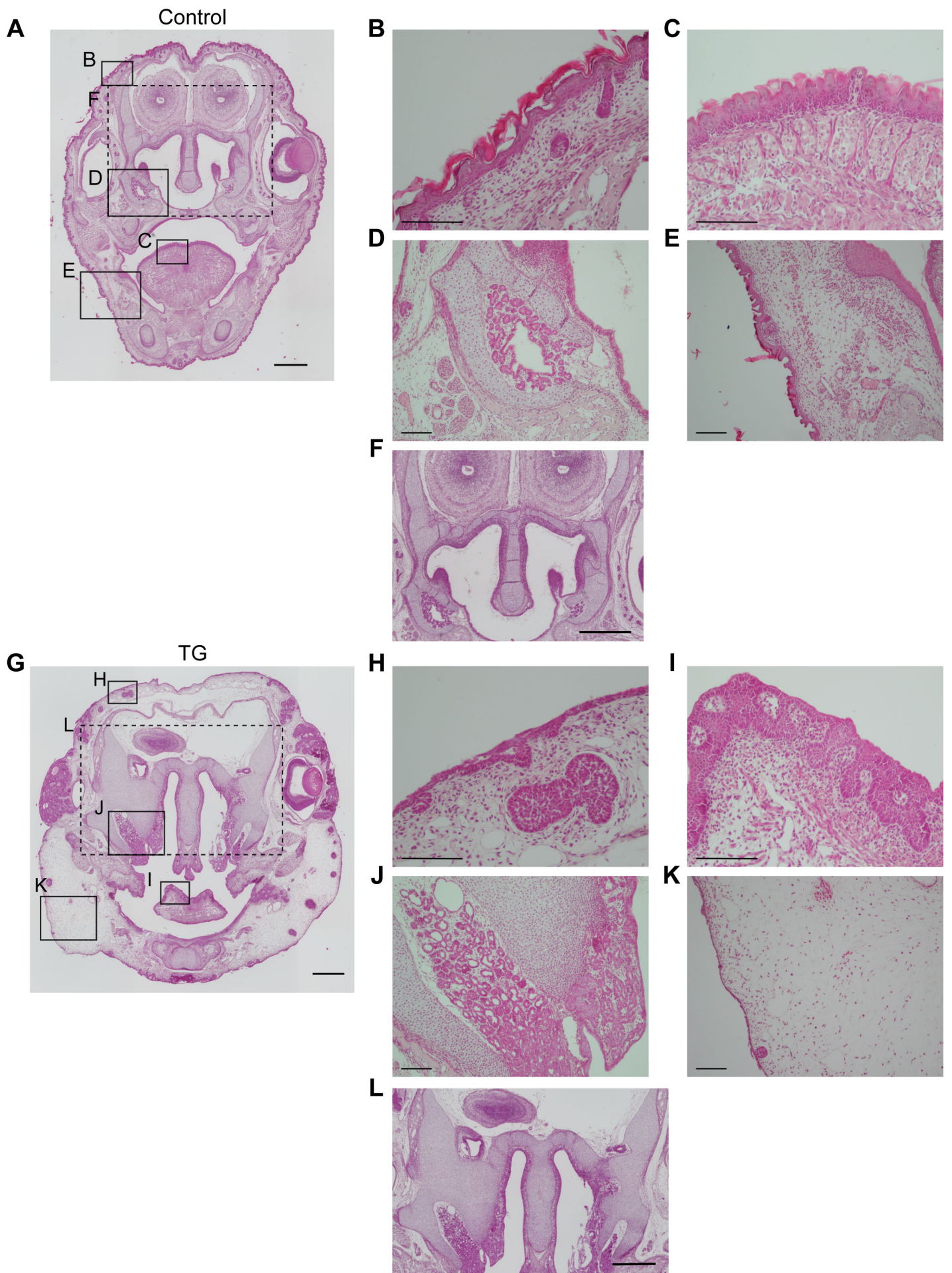
A Control   TG

B Control   TG

C Control   TG

E Control

TG

D Control   TG

Figure 1.

A

B

C

Figure 2.

A Control

B

C

D

E

F

G TG

H

I

J

K

L

Figure 3.

	Control	TG
Hematoxylin-eosin	A	E
Type X collagen	B	F
ALP	C	G
TRAP	D	H

Figure 4.

Figure 5.

A

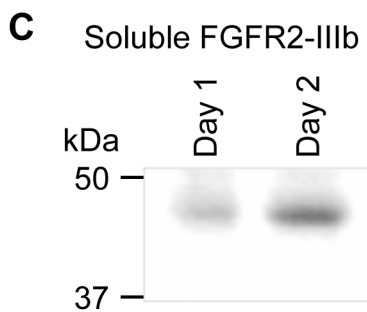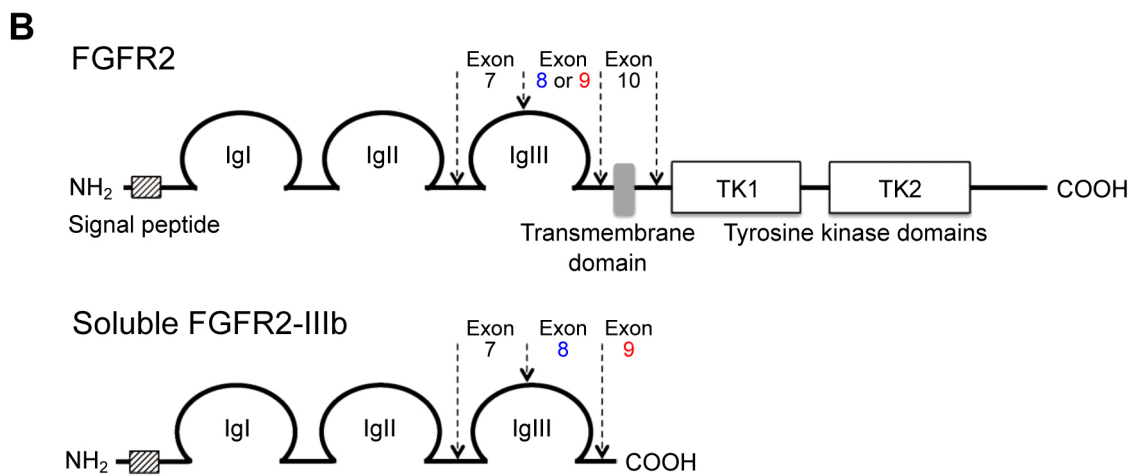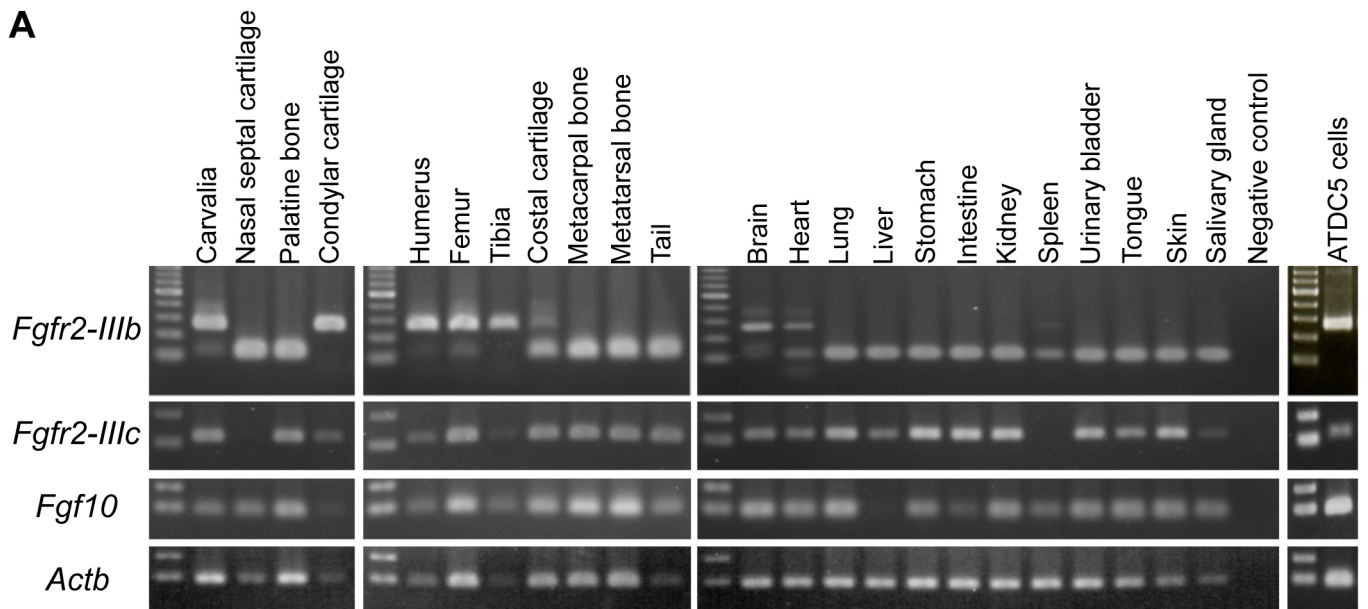**B**

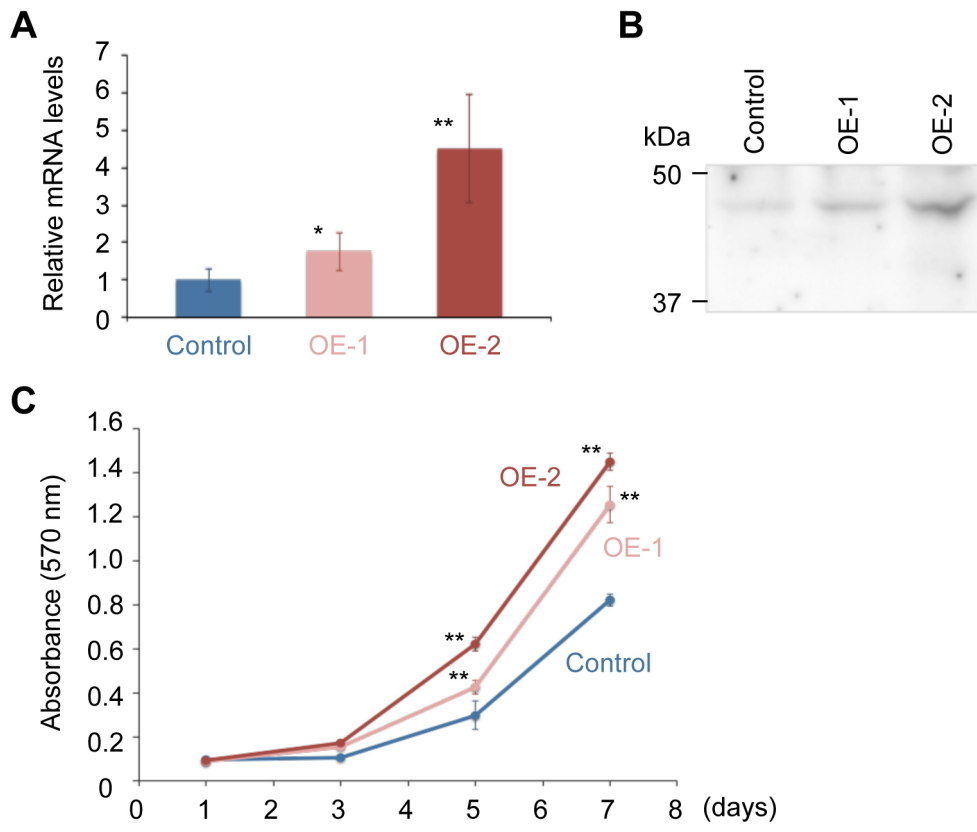**C** Soluble FGFR2-IIIb

D FGF10
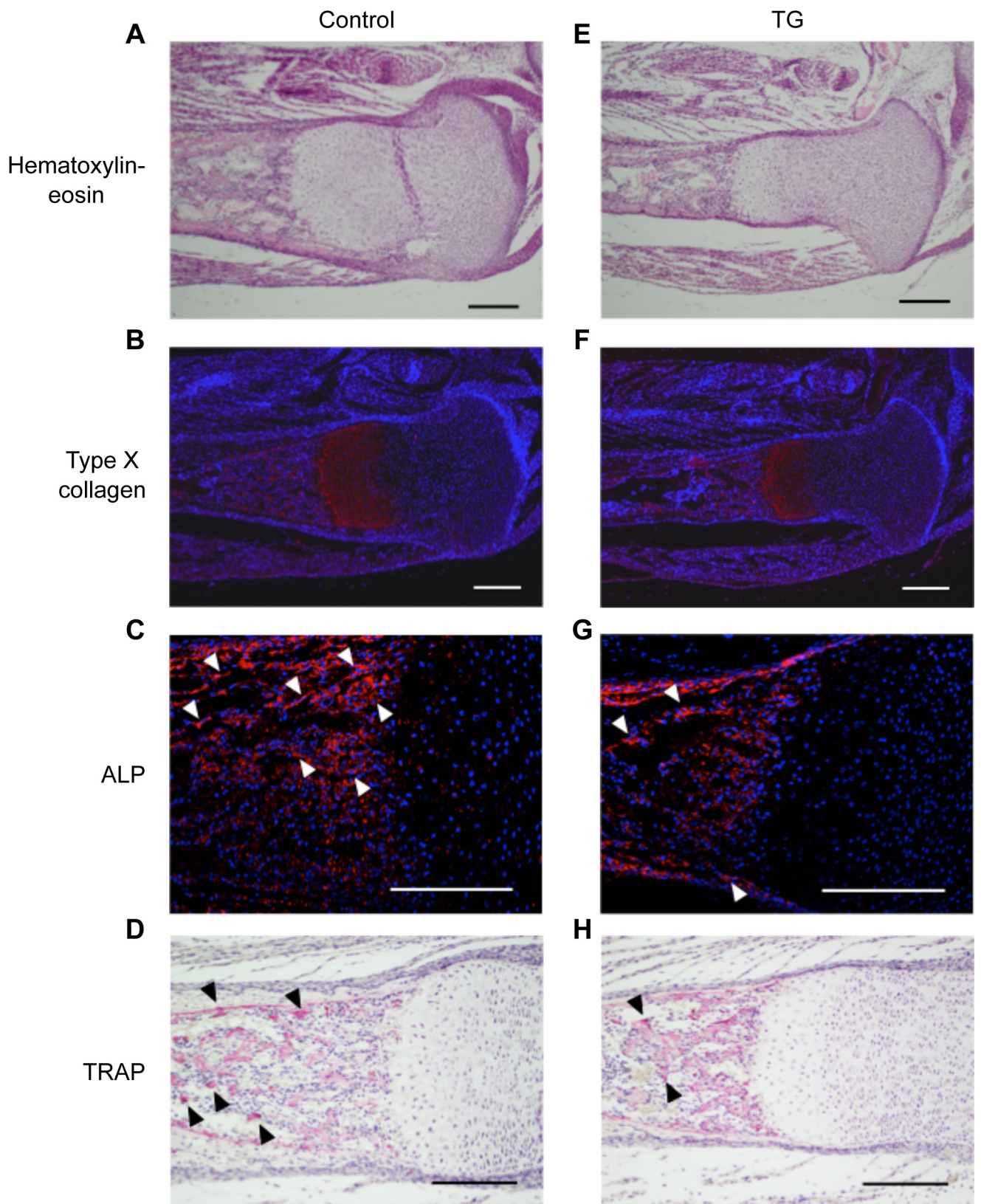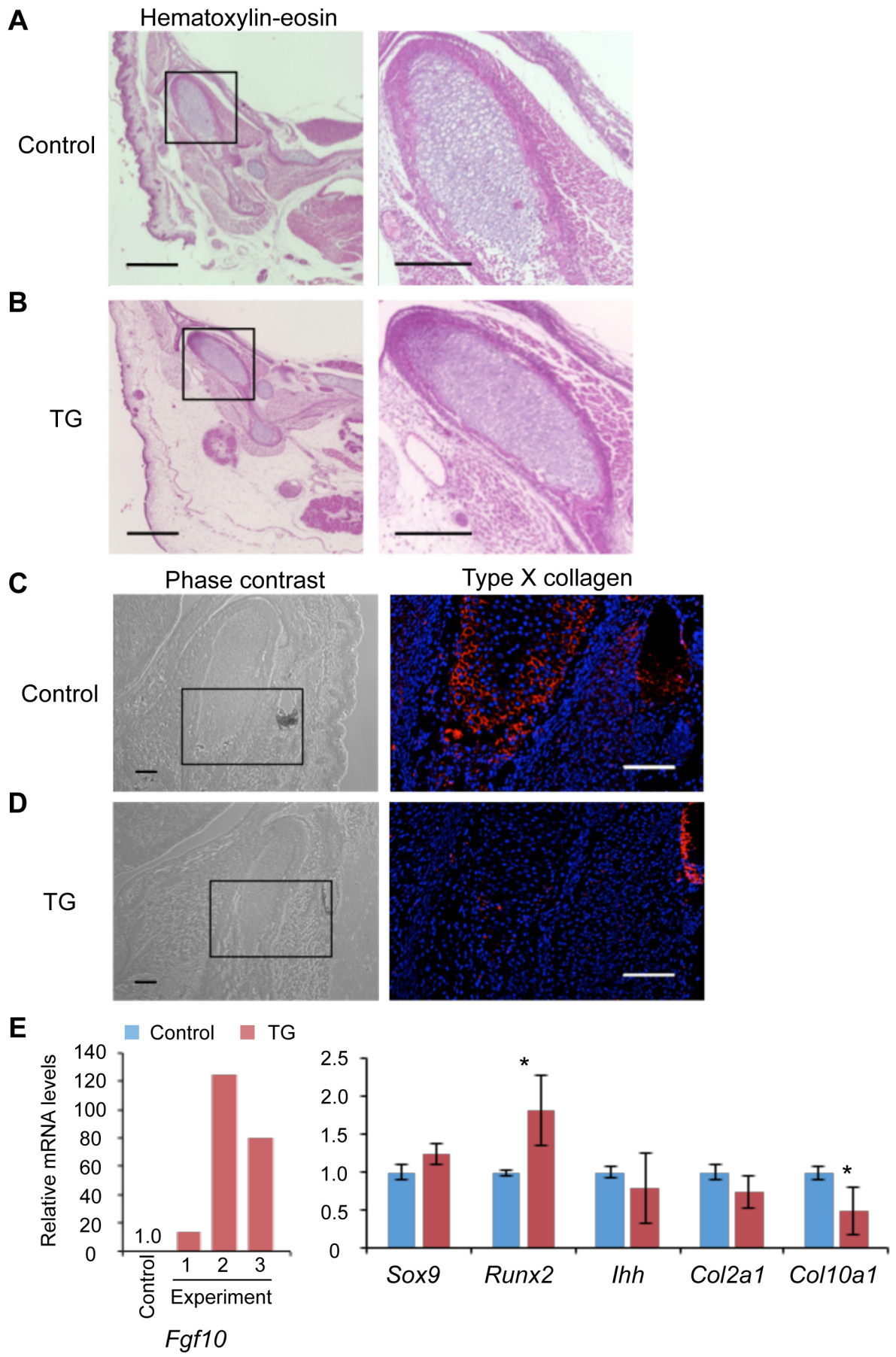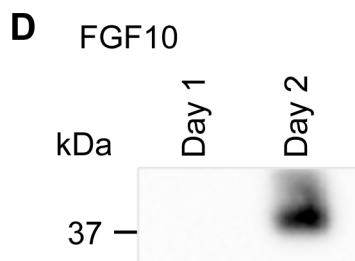
Figure 6.

Figure 7.

VIII. REFERENCES

Abzhanov A, Tabin CJ. Shh and Fgf8 act synergistically to drive cartilage outgrowth during cranial development. *Dev Biol* 2004; 273: 134-148.

Balasubramanian R, Zhang X. Mechanisms of FGF gradient formation during embryogenesis. *Semin Cell Dev Biol* 2015; in press.

Beenken A, Mohammadi M. The FGF family: biology, pathophysiology and therapy. *Nat Rev Drug Discov* 2009; 8: 235-253.

Berendsen AD, Olsen BR. Bone development. *Bone* 2015; 80: 14-18.

Clark JC, Tichelaar JW, Wert SE, Itoh N, Perl AK, Stahlman MT, Whitsett JA. FGF-10 disrupts lung morphogenesis and causes pulmonary adenomas in vivo. *Am J Physiol Lung Cell Mol Physiol* 2001; 280: L705-715.

De Moerlooze L, Spencer-Dene B, Revest JM, Hajihosseini M, Rosewell I, Dickson C. An important role for the IIIb isoform of fibroblast growth factor receptor 2 (FGFR2) in mesenchymal-epithelial signalling during mouse organogenesis. *Development* 2000; 492: 483-492.

Goetz R, Mohammadi M. Exploring mechanisms of FGF signalling through the lens of structural biology. *Nat Rev Mol Cell Biol* 2013; 14: 166-180.

Gonzaga S, Henriques-Coelho T, Davey M, Zoltick PW, Leite-Moreira AF, Correia-Pinto J, Flake AW. Cystic adenomatoid malformations are induced by localized FGF10 overexpression in fetal rat lung. *Am J Respir Cell Mol Biol* 2008; 39: 346-355.

Hajihosseini MK, Duarte R, Pegrum J, Donjacour A, Lana-Elola E, Rice DP, Sharpe J, Dickson C. Evidence that Fgf10 contributes to the skeletal and visceral defects of an Apert syndrome mouse model. *Dev Dyn* 2009; 238: 376-385.

Hinoi E, Bialek P, Chen YT, Rached MT, Groner Y, Behringer RR, Ornitz DM, Karsenty G. Runx2 inhibits chondrocyte proliferation and hypertrophy through its expression in the perichondrium. *Genes Dev* 2006; 20: 2937-2942.

Igarashi M, Finch PM, Aaronson SA. Characterization of recombinant human fibroblast growth factor (FGF)-10 reveals functional similarities with keratinocyte growth factor (FGF-7). *J Biol Chem* 1998; 273: 13230-13235.

Itoh N. FGF10: A multifunctional mesenchymal–epithelial signaling growth factor in development, health, and disease. *Cytokine Growth Factor Rev* 2015; in press.

Jacob AL, Smith C, Partanen J, Ornitz DM. Fibroblast growth factor receptor 1 signaling in the osteo-chondrogenic cell lineage regulates sequential steps of osteoblast maturation. *Dev Biol* 2006; 296: 315-28.

Kaufman MH. The atlas of mouse development. London: Academic Press; 1992.

Kimmel CA, Trammell C. A rapid procedure for routine double staining of cartilage and bone in fetal and adult animals. *Stain Technol* 1981; 56: 271-273.

Kistner A, Gossen M, Zimmermann F, Jerecic J, Ullmer C, Lübbert H, Bujard H. Doxycycline-mediated quantitative and tissue-specific control of gene expression in transgenic mice. *Proc Natl Acad Sci USA* 1996; 93: 10933-10938.

Kobayashi T, Kronenberg HM. Overview of skeletal development. *Methods Mol Biol* 2014; 1130: 3-12.

Mansour SL, Goddard JM, Capecchi MR. Mice homozygous for a targeted disruption of the proto-oncogene int-2 have developmental defects in the tail and inner ear. *Development* 1993; 117: 13-28

Marchese C, Felici A, Visco V, Lucania G, Igarashi M, Picardo M, Frati L, Torrisi MR. Fibroblast growth factor 10 induces proliferation and differentiation of human primary cultured keratinocytes. *J Invest Dermatol* 2001; 116: 623-628.

McBratney-Owen B, Iseki S, Bamforth SD, Olsen BR, Morriss-Kay GM. Development and tissue origins of the mammalian cranial base. *Dev Biol* 2008; 322: 121-132.

Ohta H, Itoh N. Roles of FGFs as adipokines in adipose tissue development, remodeling, and metabolism. *Front Endocrinol* 2014; 5: 1-4.

Olney RC, Wang J, Sylvester JE, Mougey EB. Growth factor regulation of human growth plate chondrocyte proliferation in vitro. *Biochem Biophys Res Commun* 2004; 317: 1171-1182.

Ornitz DM. FGF signaling in the developing endochondral skeleton. *Cytokine Growth Factor Rev* 2005; 16: 205-213.

Ornitz DM, Marie PJ. Fibroblast growth factor signaling in skeletal development and disease. *Genes Dev* 2015; 29: 1463-1486.

Parsa S, Kuremoto K, Seidel K, Tabatabai R, Mackenzie B, Yamaza T, Akiyama K, Branch J, Koh CJ, Al Alam D, Klein OD, Bellusci S. Signaling by FGFR2b controls the regenerative capacity of adult mouse incisors. *Development* 2010; 137: 3743-3752.

Sakaue H, Konishi M, Ogawa W, Asaki T, Mori T, Yamasaki M, Takata M, Ueno H, Kato S, Kasuga M, Itoh N.   Requirement of fibroblast growth factor 10 in development of white adipose tissue. *Genes Dev* 2002; 16: 908-912.

Sekine K, Ohuchi H, Fujiwara M, Yamasaki M, Yoshizawa T, Sato T, Yagishita N, Matsui D, Koga Y, Itoh N, Kato S. Fgf10 is essential for limb and lung formation. *Nat Genet* 1999; 21: 138-141.

Shannon JM, Hyatt BA. Epithelial-mesenchymal interactions in the developing lung. *Annu Rev Physiol* 2004; 66: 625-645.

Shimoaka T, Ogasawara T, Yonamine A, Chikazu D, Kawano H, Nakamura K, Itoh N, Kawaguchi H. Regulation of osteoblast, chondrocyte, and osteoclast functions by fibroblast growth factor (FGF)-18 in comparison with FGF-2 and FGF-10. *J Biol Chem* 2002; 277: 7493-7500.

Su N, Jin M, Chen L. Role of FGF/FGFR signaling in skeletal development and homeostasis: learning from mouse models. *Bone Res* 2014; 2: 14003.

Terao F, Takahashi I, Mitani H, Haruyama N, Sasano Y, Suzuki O, Takano-Yamamoto T. Fibroblast growth factor 10 regulates Meckel's cartilage formation during early mandibular morphogenesis in rats. *Dev Biol* 2011; 350: 337-347.

Veistinen L, Aberg T, Rice DP. Convergent signalling through Fgfr2 regulates divergent craniofacial morphogenesis. *J Exp Zool B Mol Dev Evol* 2009; 312B: 351-360.

Wang F, Kan M, McKeehan K, Jang JH, Feng S, McKeehan WL. A homeo-interaction sequence in the ectodomain of the fibroblast growth factor receptor. *J Biol Chem* 1997; 272: 23887-23895.

White KE, Cabral JM, Davis SI, Fishburn T, Evans WE, Ichikawa S, Fields J, Yu X, Shaw NJ, McLellan NJ, McKeown C, Fitzpatrick D, Yu K, Ornitz DM, Econs MJ. Mutations that cause osteoglophonic dysplasia define novel roles for FGFR1 in bone elongation. *Am J Hum Genet* 2005; 76: 361-367.

Yang L, Tsang KY, Tang HC, Chan D, Cheah KS. Hypertrophic chondrocytes can become osteoblasts and osteocytes in endochondral bone formation. *Proc Natl Acad Sci USA* 2014; 111: 12097-12102.

Yoshida CA, Yamamoto H, Fujita T, Furuichi T, Ito K, Inoue K, Yamana K, Zanma A, Takada K, Ito Y, Komori T. Runx2 and Runx3 are essential for chondrocyte maturation, and Runx2 regulates limb growth through induction of Indian hedgehog. *Genes Dev* 2004; 18: 952-963.

Zhang X, Ibrahimi OA, Olsen SK, Umemori H, Mohammadi M, Ornitz DM. Receptor specificity of the fibroblast growth factor family. The complete mammalian FGF family. *J Biol Chem* 2006; 281: 15694-15700.

Zheng Q, Zhou G, Morello R, Chen Y, Garcia-Rojas X, Lee B. Type X collagen gene regulation by Runx2 contributes directly to its hypertrophic chondrocyte-specific expression in vivo. *J Cell Biol* 2003; 162: 833-842.

Zhou X, von der Mark K, Henry S, Norton W, Adams H, de Crombrugghe B. Chondrocytes transdifferentiate into osteoblasts in endochondral bone during development, postnatal growth and fracture healing in mice. *PLoS Genet* 2014; 10: e1004820.